Journal of Power Sources 246 (2014) 696–702

Contents lists available at ScienceDirect

Journal of Power Sources

journal homepage: www.elsevier.com/locate/jpowsour

# Monodispersed $LiFePO_4$@C core–shell nanostructures for a high power Li-ion battery cathode

Gang Xu [a,b], Feng Li [a,b], Zhihong Tao [a,b], Xiao Wei [a,b,*], Yong Liu [a,b], Xiang Li [a,b], Zhaohui Ren [a,b], Ge Shen [a,b], Gaorong Han [a,b,*]

[a] State Key Laboratory of Silicon Materials and Department of Materials Science and Engineering, Zhejiang University, Hangzhou 310027, China
[b] Key Laboratory of Advanced Materials and Applications for Batteries of Zhejiang Province, Hangzhou 310027, China

## HIGHLIGHTS

- Monodispersed $LiFePO_4$ nanopillows were solvothermally synthesized with ethylene glycol.
- $LiFePO_4$@C core–shell nanostructures were prepared by a facile method in high yield.
- LiFePO4@C core–shell nanostructures show nice capacity retention and high rate capacity.
- A facile method was proposed simply to prepared fully carbon-coated $LiFePO_4$ cathode.

## GRAPHICAL ABSTRACT

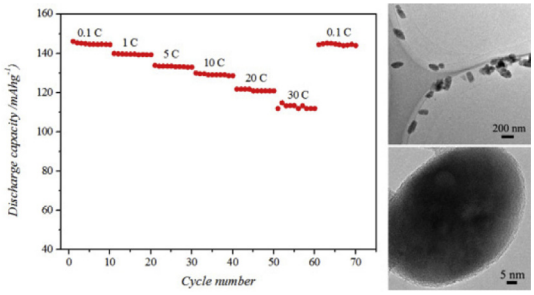


## ARTICLE INFO

*Article history:*
Received 27 May 2013
Received in revised form
20 July 2013
Accepted 24 July 2013
Available online 20 August 2013

*Keywords:*
Lithium iron phosphate
Solvothermal route
Core–shell nanostructures
Carbon-coating
Cathode materials
Li-ion battery

## ABSTRACT

In this paper, monodispersed $LiFePO_4$ nanopillows have been successfully synthesized via solvothermal route with ethylene glycol (EG) as reaction medium. Subsequently, with the basis of the solvothermally synthesized monodispersed $LiFePO_4$ nanopillows, monodispersed $LiFePO_4$@C core–shell nanostructures are facilely prepared in high yield. Based on the experimental results, the formation mechanism of the monodispersed $LiFePO_4$ nanopillows has been discussed simply. The monodispersed $LiFePO_4$@C core–shell nanostructures exhibit nice capacity retention and high rate capacity due to the full carbon-coating and the well-crystallized nanosized particles.



## 1. Introduction

Over the past decade, tremendous efforts have been performed to find alternatives to the toxic and expensive cathodes currently employed in commercialized lithium-ion batteries, such as cobalt-oxide-based materials. As an alternative, the ordered olivine lithium iron phosphate, $LiFePO_4$, has been intensively investigated since the pioneering work of Padhi et al. [1]. Moreover, $LiFePO_4$ is regarded as the most promising cathode materials for power

* Corresponding authors. State Key Laboratory of Silicon Materials and Department of Materials Science and Engineering, Zhejiang University, Hangzhou 310027, China. Tel./fax: +86 571 87952341.
*E-mail addresses:* mseweixiao@zju.edu.cn (X. Wei), hgr@zju.edu.cn (G. Han).

0378-7753/$ – see front matter © 2013 Elsevier B.V. All rights reserved.
http://dx.doi.org/10.1016/j.jpowsour.2013.07.089

batteries used in electric vehicles (EVs) and hybrid electric vehicles (HEVs), due to the moderate flat voltage plateau (3.4 V versus $Li^+/Li$), high theoretical specific capacity (170 mAh $g^{-1}$), intrinsic thermal safety, environmental compatibility, and abundance of iron resources in nature [2,3]. However, the rate performance of the original $LiFePO_4$ was significantly restricted by sluggish kinetics of electron and lithium-ion transport [4–7]. Thus, enormous attempts have been carried out to improve the rate performance by enhance the conductivity, including surface coating or admixing with carbon and other electronically conductive materials [8–11], reducing particle size and controlling morphology [10,12], and doping with isovalent or supervalent cations [5,6,13,14].

In recent years, some works on the modification of $LiFePO_4$ particles represent significant progresses in the improvement of the rate performance. Wang et al. reported that a core–shell $LiFePO_4$ nanocomposite prepared by an in situ polymerization restriction method could present a capacity of 90 mAh $g^{-1}$ at rate of 60 C [10]. Wu et al. suggested that a nanocomposite with highly dispersed $LiFePO_4$ nanoparticles in a nanoporous carbon matrix couple discharge at a rate up to 230 C [15]. Zhou et al. also illustrated that a nanocomposite, in which the $LiFePO_4$ primary nanoparticles are wrapped homogeneously and loosely with a graphene 3D network, could deliver a capacity of 70 mAh $g^{-1}$ at 60 C discharge rate [9]. All the above-mentioned reports demonstrated that full coating with carbon [10] is essential to attain high electrochemical performance. However, we know that the approaches based on the thermal decomposition of carbon-containing precursors, which have been widely used for the preparation of carbon-coated $LiFePO_4$ particles [8–10,16–20], generally involve a high temperature treatment for forming carbon-coating. Due to the agglomeration of the $LiFePO_4$ nanoparticles and the crystal further growth occurred during the high temperature treatment, only partial surface of the $LiFePO_4$ particles is coated with the conductive carbon [10,20]. Whereas the full carbon-coating facilitates the high power batteries, it is essential to pursue the preparation of the full carbon-coated $LiFePO_4$ nanoparticles in high yield.

The popular strategy to synthesize $LiFePO_4$ is the solid state reaction route performed at high temperature under inert atmosphere. Frequently, a few impurities, such as $Li_3Fe_2(PO_4)_3$, $Fe_2O_3$, and $LiPO_4$, are involved in the final products [21,22]. Moreover, due to the calcinations at high temperature it is also very difficult to obtain fine and homogeneous particles. In order to obtain $LiFePO_4$ with fine particles for high rate performance and high capacity, it is essential to take advantage of solution synthetic route, such as precipitation [23], sol–gel [24,25], polyol [26,27], and hydrothermal reaction route [8,11,13,28–31]. Among these methods, hydrothermal reaction receives particular attention due to the mild operation temperature, well crystallization, simple process and low cost. Otherwise, hydrothermal reaction can be easily tailored to produce nanostructures by the modulation of reaction temperature, concentration of precursors, reaction medium solvent, and the addition of organic compounds [32,33]. In a pioneering attempt, Whittingham et al. have successfully realized the synthesis of $LiFePO_4$ via hydrothermal reaction route [28,29]. Due to severe displacement of Fe in Li site, the products hydrothermally synthesized at 120 °C show low electrochemical activity. With the hydrothermal treatment temperature increasing above 180 °C, the displacement of Fe in Li site can be remarkably suppressed. However, probably due to the particle size enlargement or the presence of impurities brought about from the oxidation of Fe(II) salt the electrochemical activity improves slightly [29,30]. Subsequent works have shown that the impurities can be avoided by introducing some organic reagents, such as ascorbic acid, polyacrylic acid, and citric acid, to prevent the oxidation of Fe(II) to Fe(III) [8,13,16,31].

Recently, a novel hydrothermal system, in which the ethylene glycol (EG) was used with water or other organic reagents as the reaction medium, has been developed to prepare size- and morphology-controlled $LiFePO_4$ nanostructures for improving the electrochemical properties [12,34–37]. Rangappa et al. [34] reported that $LiFePO_4$ nanorods and hierarchical flower-like microstructures have been synthesized via solvothermal reaction route by employing EG with hexane or oleic acid as reaction medium solvent. Teng et al. [35] solvothermally synthesized the $LiFePO_4$ nanodendrites by employing EG/water mixture solvent as reaction medium assisted with the surfactant of dodecyl benzene sulphonic acid sodium (SDBS). As anodized alumina oxide (AAO) is used as template in the hydrothermal reaction system, the preparation of $LiFePO_4$ nanorod arrays is also realized via hydrothermal method with EG and water mixture solvent as reaction medium [36]. More recently, Goodenough et al. [12] develop a novel solvothermal approach, in which EG and ethylenediamine mixture solvent was used as reaction medium, combined with high temperature calcinations to synthesize $LiFePO_4$ microspheres with an open three-dimensional (3D) porous microstructure in a large scale. These porous $LiFePO_4$ microspheres show excellent rate capability and cycle stability. Obviously, the EG plays an important role in the morphology-controlled synthesis of $LiFePO_4$ particle for improving the electrochemical properties mentioned above. During the synthesis processes, EG not only as a stabilizer suppresses the particle growth and the agglomeration but also as a reducer suppresses the oxidation of Fe(II) [12].

Herein we report a facile process for the preparation of the monodispersed $LiFePO_4$@C core–shell nanostructures in high yields, in which carbon-coating fully covers the highly crystalline monodispersed $LiFePO_4$ nanopillows with a size of ca. 100 nm in diameter and ca. 100–200 nm in length. As shown in Scheme 1, our strategy includes two steps: one is the synthesis of the monodispersed $LiFePO_4$ nanopillows via a simple solvothermal reaction route with ethylene glycol as reaction medium solvent under the effect of ascorbic acid as reducer, and the second is the full carbon-coating realized by dispersing the obtained monodispersed $LiFePO_4$ nanopillows in ascorbic acid solution and following high temperature decomposition after drying. Due to the high perfect crystallization and the full carbon-coating, the monodispersed $LiFePO_4$@C core–shell nanostructures exhibit nice capacity retention and high rate capacity.

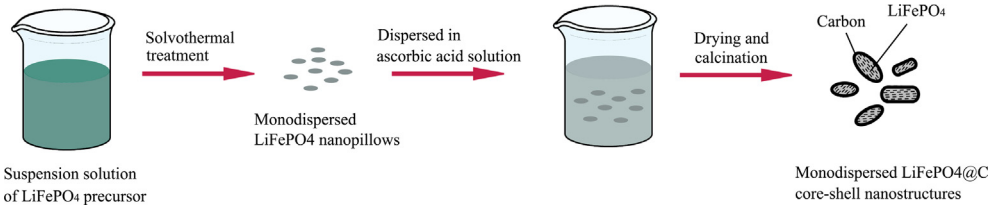


**Scheme 1.** Schematic representation of the preparation of the monodispersed $LiFePO_4$@C core–shell nanostructures.

## 2. Experimental

The solvothermal reaction was carried out in a home-made Telflon-lined stainless steel autoclave. All the chemicals are of analytical grade and were used as purchased without further purification. $FeSO_4{\cdot}7H_2O$, $LiOH{\cdot}H_2O$ and $H_3PO_4$ (85 wt%) were purchased from Shanghai Chemical Reagent Factory (Shanghai, China), ethylene glycol (EG) from Tianjin Damao Chemical reagent Factory (Tianjin, China), ascorbic acid from Alfa Aesar (Shanghai, China), respectively.

Monodispersed $LiFePO_4$ nanoparticles were synthesized by a simple solvothermal route with EG as the reaction medium solvent. In a typical procedure, appropriate quantities of $FeSO_4{\cdot}7H_2O$ and $H_3PO_4$ were together added into EG, forming a mixed transparent solution with absinthe-green, and appropriate quantities of $LiOH{\cdot}H_2O$ was dissolved in EG, forming a transparent LiOH solution. In order to prevent the oxidation of Fe(II), a desired amount of ascorbic acid was added into the mixed solution. Then, the mixed solution was introduced dropwise into the LiOH under the vigorous magnetic stirring, forming an absinthe-green suspension with a lot of precipitates. After stirring for 30 min, the consequent absinthe-green suspension as feedstock was transferred into a 50 mL Teflon-lined stainless steel autoclave and occupied about 40 mL. In the final feedstock suspension, the $Li^+$, $Fe^{2+}$, $PO_4^{3-}$ and ascorbic acid molar ratio was designed as 3:1:1:1. The solvothermal treatment was performed by placing the sealed autoclave in an oven and keeping it at 230 °C for 6 h. After being cooled to room temperature in air, the products were centrifuged and washed several times with distilled water and absolute alcohol. In order to improve the rate performance and capacity, the washed and centrifuged products were dispersed in ascorbic acid aqueous solution and followed by being dried at 80 °C for 12 h heat treated at 600 °C for 6 h under $N_2$ atmosphere for coating a carbon film on the surface of the $LiFePO_4$ particles. As a control experiment, $LiFePO_4$ was also prepared by a hydrothermal route, in which distilled water was used as reaction medium instead of EG.

X-ray powder diffraction (XRD) patterns were collected by a Rigaku D/max-RA X-ray diffractometer with Cu Kα ($\lambda = 1.5418$ Å) radiation with a step size of 0.02°. Field-emission scanning electron microscopy (FESEM) measurements were performed using a Hitachi S-400 microscope (Japan). High-resolution transmission electron microscopy (HRTEM) images were obtained by an FEI Tecnai G2 F30 TEM with an acceleration voltage of 200 kV. Malvern mastersizer 2000 laser particle size analyzer was used to analyze the particle size distribution of the synthesized samples. Thermogravimetric analysis (TG) performed with an NETZSCH TG 209 thermal analyzer was employed to identify the amount of the coated carbon from room temperature to 700 °C as a heating rate of 10 °C $min^{-1}$ in air.

The electrochemical properties of the $LiFePO_4$ samples were evaluated by assembling CR2025 coin-type cells in an argon-filled glove box. The prepared $LiFePO_4$ samples with carbon coated were dried at 100 °C for 12 h in a vacuum desiccator before assembling the cell. After drying, the dried $LiFePO_4$ samples were mixed with acetylene black and polyvinylidene fluoride (PVDF) binder in the weight ratio of 75:15:10 by blending in *N*-methylpyrrolidone. The prepared slurry was coated on an aluminum foil discs with a loading of ca. 2 mg $cm^{-2}$ and dried using as cathode. Lithium foil was used as counter electrode and LB 301 $LiPF_6$ solution (gotten from Guotaihuarong Zhangjiagang, China) as electrolyte, respectively. A Teflon Celgard separator (#2400) was used to separate the working electrode and the lithium foil counter electrode. Charge/discharge test of the assembled coin cell was carried out with a BTS 5V1A system (Neware Shenzhen, China) under different current densities in the voltage range of 2.0–4.2 V at 25 °C. Cyclic voltammogram (CV) tests (scan rate of 0.1 mV $S^{-1}$ in the voltage range of 2.0–4.2 V) were performed by an electrochemical workstation CHI604D (Chenhua, Shanghai, China).

## 3. Results and discussion

Fig. 1 shows the XRD patterns of the hydrothermally and ethylene glycol (EG) solvothermally synthesized samples. All the diffraction peaks caught from the both powders can be indexed to the orthorhombic lattice of $LiFePO_4$ (JCPDS no. 81-1173), indicating that the both powders are of pure crystalline $LiFePO_4$ crystals with olivine structure. The strong and sharp reflection peaks suggest that the as-prepared $LiFePO_4$ products are well crystallized. Otherwise, compared in detail one can find that the diffraction intensity of the hydrothermally synthesized powders is stronger than that of the EG-solvothermally synthesized. Thus, it is reasonable to infer that the hydrothermally synthesized $LiFePO_4$ is of larger particle than that synthesized by solvothermal method with EG as the reaction medium.

Fig. 2a–c presents the SEM and TEM images of the hydrothermally and EG-solvothermally synthesized $LiFePO_4$ powders. The hydrothermally synthesized sample is of irregular particles with a size of about 200–500 nm and severe agglomeration, whereas the solvothermally synthesized with EG as reaction medium solvent is almost composed of nanopillows with size narrow distribution of about 100 nm in diameter and 100–200 nm in length and good monodispersibility. The TEM image shown in Fig. 2c and the particle size distribution profile shown in Fig. 2d further illustrate the good monodispersibility of the solvothermally synthesized $LiFePO_4$ nanopillows. The particle size of the solvothermally synthesized LiFePO4 nanopillows distributes in a narrow range around 180 nm, very consistent with the observed results of SEM and TEM (Fig. 2b and c). With the base of the experimental results above, it can be concluded that EG is essential for formation of the monodispersed $LiFePO_4$ nanopillows.

It is well known that the formation of nanocrystals involves two steps: nucleation and growth. According to the formation mechanism of oxides under hydrothermal conditions [38], at the initial stage of the hydrothermal reaction the precursors dehydrate and condensate to form $LiFePO_4$ species under the high temperature and the autogenetic pressure. When the $LiFePO_4$ species accumulate to a moderate concentration, a number of nuclei larger than the critical size appear. These nuclei then grow by incorporating the

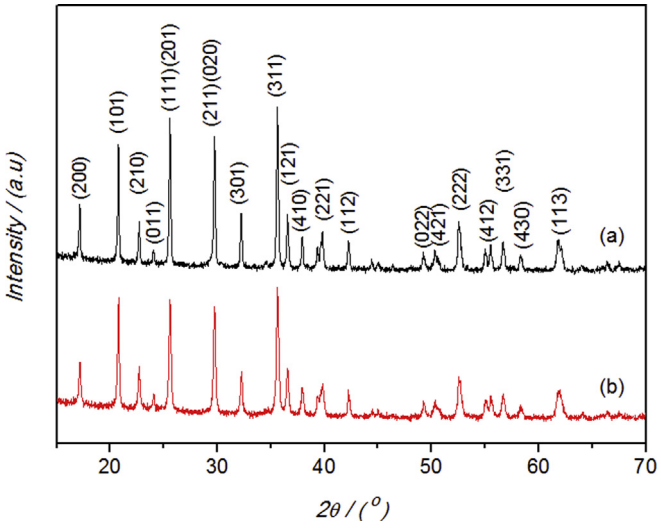


**Fig. 1.** X-ray diffraction patterns of the (a) hydrothermally, and (b) ethylene glycol solvothermally synthesized $LiFePO_4$ samples.

additional $LiFePO_4$ species to form $LiFePO_4$ crystals. We know that crystal growth in an aqueous medium follows an Ostwald ripening process. Due to the fact that the $LiFePO_4$ species concentration around the smaller particles is higher than that around the bigger particles, the bigger merge the smaller. Thus, the hydrothermally synthesized $LiFePO_4$ crystals grow to of a larger size of 200–500 nm. Moreover, due to the strong polarity of the water molecules the hydrothermally synthesized $LiFePO_4$ crystals agglomerate severely (Fig. 2a).

Previous experimental researching work has demonstrated that the water involved in the reaction feedstock is essential to realize the formation of the oxide crystals synthesized by solvothermal reaction route. Due to the absence of water, after undergoing a solvothermal treatment at 200 °C, the mixed lead acetylacetonate, titanium and zirconium alkoxides in 2-butanone only produce amorphous powders without any $PbTiO_3$, $Pb(Zr,Ti)O_3$, and $PbZrO_3$ crystals formed [39]. However, in the present experiment, due to the introduction of the raw materials of $FeSO_4 \cdot 7H_2O$, $LiOH \cdot H_2O$ and $H_3PO_4$ (85 wt%), a little water were involved in the solvothermal reaction system although only EG is used as solvent to make the feedstock. The existence of the little water makes the dehydrating condensation of the $LiFePO_4$ precursors and results in the crystallization of $LiFePO_4$ olivine (Fig. 1a). Whereas the volume fraction of the involved water in the feedstock is very small and a lot of $LiFePO_4$ precursors take part in the dehydrating condensation, it can be inferred that in the initial stage of the solvothermal treatment the local concentration of the formed $LiFePO_4$ species accumulates high. Moreover, we know that high concentration of species facilitates a fast nucleation and a large number of crystal nuclei for growing. These nuclei then grow by incorporating additional species still present in the reaction medium. Whereas the precursors for dehydrating condensation to $LiFePO_4$ species are definite, the large numbers of nuclei grow to $LiFePO_4$ nanopillows with regular shape and a narrow distribution. Otherwise, EG, which is an organic solvent and has two hydroxyls in the molecular conformation, easily adsorbs on the formed $LiFePO_4$ nanocrystallites by hydrogen bonds. The adsorption of EG further inhibits the growth of the $LiFePO_4$ crystals. The cooperation of the poured nucleation brought about from the small volume fraction of the water involved in the feedstock and the adsorption of EG result in the synthesis of the $LiFePO_4$ nanopillows with narrow distribution (Fig. 2b). Furthermore, due to the adsorption of EG, the synthesized $LiFePO_4$ nanopillows are of good monodispersibility (Fig. 2c). Compared with the reported by Li et al. [37], it is believed that the increase of the introduced $LiOH \cdot H_2O$ in the feedstocks (the mole ratio of $FeSO_4 \cdot 7H_2O$, $H_3PO_4$ and $LiOH \cdot H_2O$ from 1:1:2.7 to 1:1:3.0) and the introduction of the ascorbic acid contribute to the morphology evolution of the synthesized $LiFePO_4$ particles from nanoplates to nanopillows.

Before the electrochemical measurements, the as-prepared $LiFePO_4$ products were firstly dispersed in ascorbic acid aqueous solution and then after drying calcined at 600 °C in inert atmosphere for forming carbon-coating. Fig. 3 exhibits the TEM and HRTEM images of the carbon-coated monodispersed $LiFePO_4$ nanopillows. The TEM image shown in Fig. 3a clearly reveals that after carbon-coating the $LiFePO_4$ nanopillows still preserve well monodispersibility. From the HRTEM image with low magnification shown in Fig. 3b, one can evidently observed that because of the well monodispersibility, the whole surfaces of the $LiFePO_4$ nanopillows are full covered with amorphous carbon-coating characterized by Raman spectra (Supporting information). The HRTEM image with high magnification shown in Fig. 3c further reveals that the thickness of the full carbon-coating is about 2.1 nm. Otherwise, the clear lattice fringes shown in the HRTEM demonstrate the core

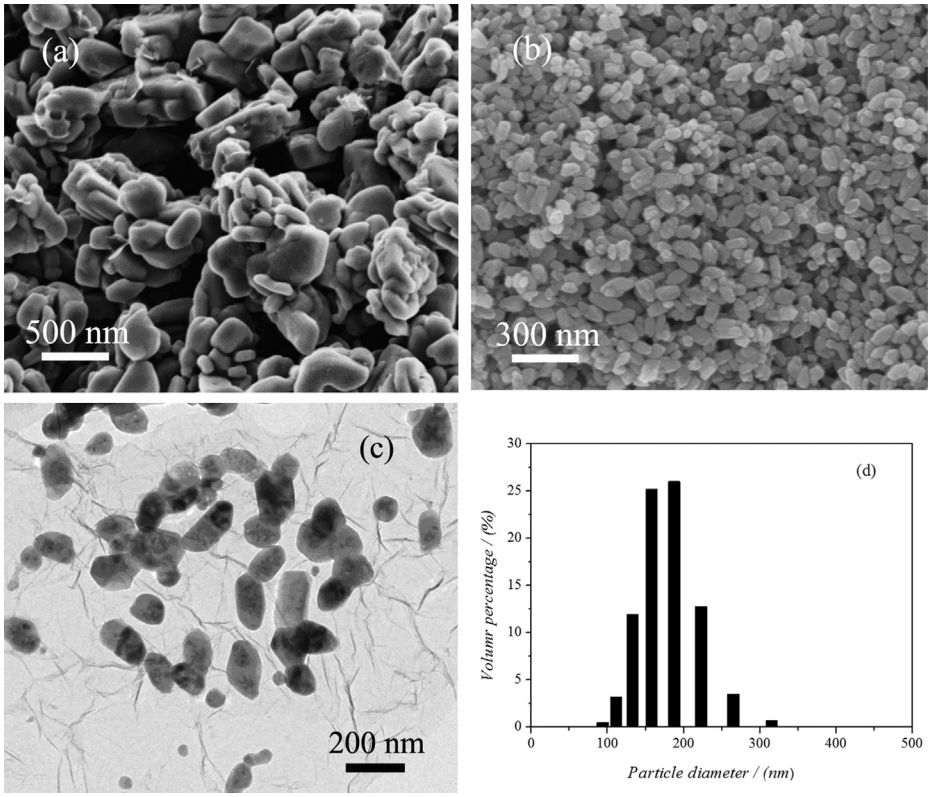


**Fig. 2.** Scanning electron microscopy images of the (a) hydrothermally, and (b) solvothermally synthesized $LiFePO_4$ samples, (c) transmission electron microscopy image of the solvothermally synthesized $LiFePO_4$ samples, and (d) particle size distribution profiles of the solvothermally synthesized $LiFePO_4$ samples.

encapsulated within the carbon-coating is composed of $LiFePO_4$ with perfect olivine crystal structure. The 0.516 nm interval between the lattice fringes agrees well with the crystal plane spacing of (200). The above measurement results manifest that after carbon-coating treatment the monodispersed $LiFePO_4$ nanoparticles are still pure $LiFePO_4$ olivine phase (JCPDS card no. 81-1173) and encapsulated by carbon-coating, forming a $LiFePO_4$@C core–shell nanostructure.

The amount of the coated carbon on the $LiFePO_4$ samples was checked by TG analysis, the results are shown in Fig. 3d. The strong weight loss occurred in the temperature range of 350–550 °C can be attributed to the combustion of the coated carbon on the $LiFePO_4$ samples. The percentage of the coated carbon in $LiFePO_4$@C core–shell nanostructures is ca. 7.30 wt%, whereas, 6.28 wt% in $LiFePO_4$/C composites prepared from the hydrothermally synthesized $LiFePO_4$ samples. It is evident that the monodispersibility and the nanosize make the $LiFePO_4$ nanopillows adsorbing more amounts of carbon than the hydrothermally synthesized $LiFePO_4$ samples.

In order to examine the potential application, the electrochemical properties of the monodispersed $LiFePO_4$@C core–shell structures were tested in CR2025 coin-type cells at 25 °C. As a contrast, the electrochemical properties of the hydrothermally synthesized $LiFePO_4$ after undergoing a same carbon-coating process ($LiFePO_4$/C composites) were also measured by assembling CR2025 coin-type cells. All the collected data, charge/discharge-specific capacities, and cyclic voltammetry curves, shown below are based on the mass of the active materials, $LiFePO_4$@C core–shell nanostructures and $LiFePO_4$/C composites. Fig. 4 presents the electrochemical performance of the monodispersed $LiFePO_4$@C core–shell structures and $LiFePO_4$/C composites. As shown in Fig. 4a, a couple of redox peaks are observed between 3.37 and 3.51 for $LiFePO_4$@C, 3.33 and 3.54 V (vs. $Li/Li^+$) for $LiFePO_4$/C, respectively, in the first cyclic voltammetry curve obtained at a scan rate of 0.5 mV $s^{-1}$. These peaks correspond to the extraction and insertion of lithium ions. The redox peaks of $LiFePO_4$@C are obviously much higher than that of $LiFePO_4$/C composites. According to the Randles–Sevcik equation [18], it can be argued that the $Li^+$ ion diffusion in $LiFePO_4$@C is fast than that in $LiFePO_4$/C composites.

Fig. 4b shows the first charge/discharge profiles of $LiFePO_4$@C and $LiFePO_4$/C at a low current rate of 0.1 C in the voltage window of 2.0–4.2 V. A long flat plateau, which corresponding to the two-phase reaction $LiFePO_4 \leftrightarrow (1-x)\,LiFePO_4 + x\,FePO_4 + x\,Li^+ + x\,e^-$, is observed from the both samples. Obviously, the charge and discharge capacities brought about from the two-phase reaction predominate. However, the discharge capacity of $LiFePO_4$@C (ca. 145 mAh $g^{-1}$) is much bigger than that of $LiFePO_4$/C composites (ca. 118.32 mAh $g^{-1}$). Otherwise, the discharge flat plateau of $LiFePO_4$@C is very close to the charge flat plateau with a small voltage difference of ca. 13 mV, whereas an obvious voltage difference of ca. 51 mV between the charge and discharge flat plateau occurs for $LiFePO_4$/C. Thus, in comparison with the $LiFePO_4$/C composites, the monodispersed $LiFePO_4$@C core–shell structures are of very small polarization, which is also revealed by the cyclic voltammetry curve

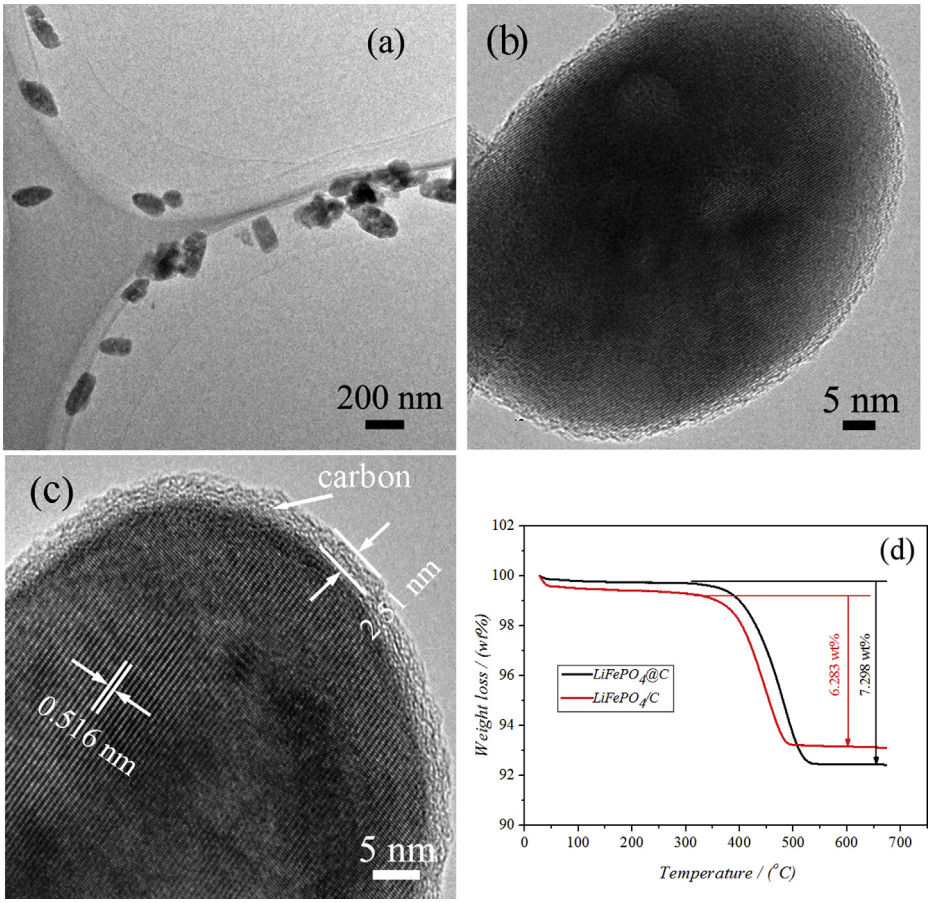


**Fig. 3.** (a) TEM image and (b) and (c) high-resolution TEM images of the monodispersed $LiFePO_4$@C core–shell nanostructures brought about from the solvothermally synthesized monodispersed $LiFePO_4$ nanopillows by undergoing a carbon-coating process with ascorbic acid as carbon-containing precursor, (d) TG curves of the carbon-coated $LiFePO_4$ samples.

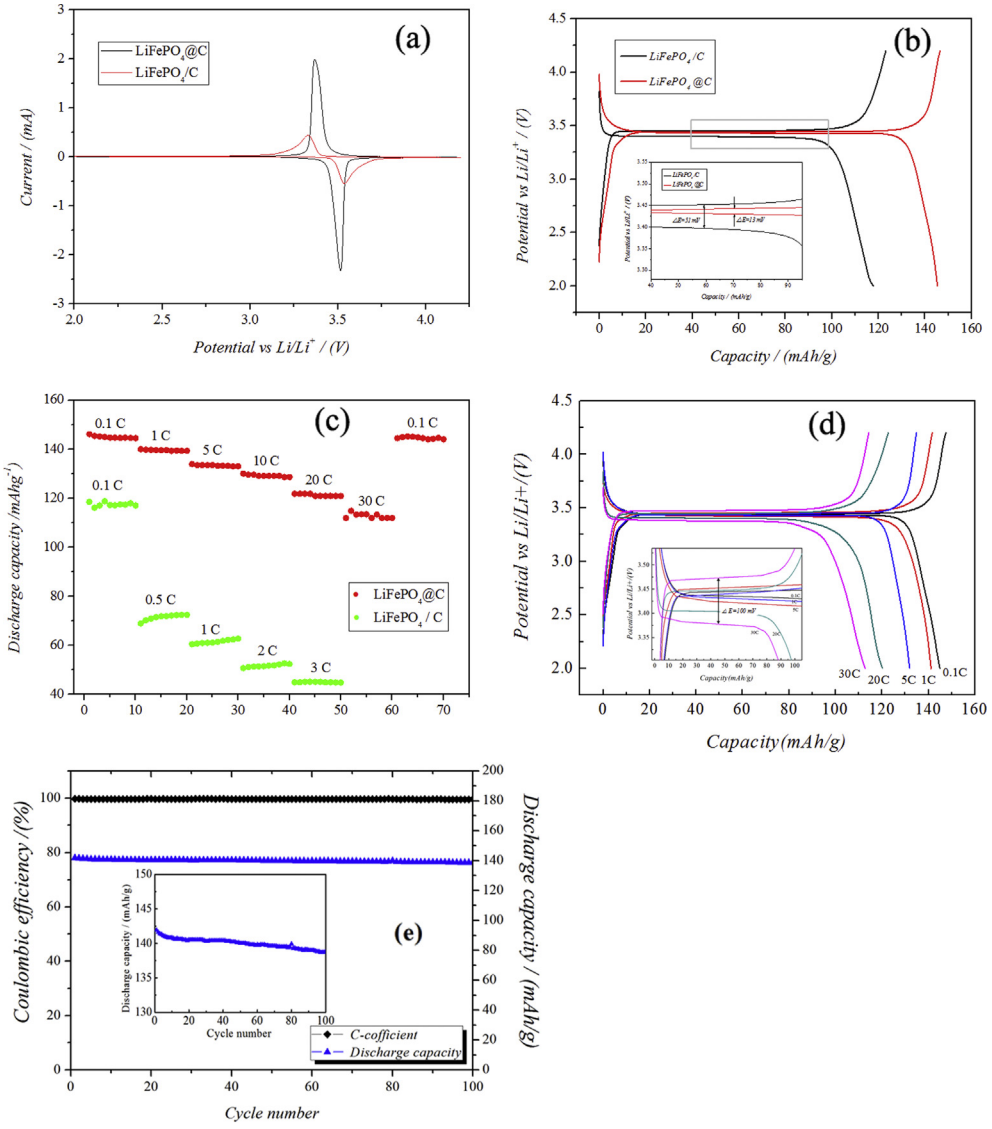


**Fig. 4.** (a) First cyclic voltammogram curves, (b) first charge–discharge profiles, and (c) comparison of rate capacity of the monodispersed $LiFePO_4$@C core–shell nanostructures and the $LiFePO_4$/C composites prepared based on the EG-solvothermally synthesized monodispersed $LiFePO_4$ nanopillows and the hydrothermally synthesized $LiFePO_4$ powders, respectively. (d) Charge–discharge profiles of $LiFePO_4$@C at different rate of 0.1, 1, 5, 20, and 30 C, (e) cycling performance and coulombic efficiency of the cell with the monodispersed $LiFePO_4$@C core–shell nanostructures as cathode at rate of 1 C.

shown in Fig. 4a, indicating that the kinetics of the $LiFePO_4$@C core–shell structures excels $LiFePO_4$/C composites.

The remarkable advantage of the monodispersed $LiFePO_4$ core–shell nanostructures is the retention of an excellent rate capability and cyclability with an improved volumetric energy density. Fig. 4c shows the comparison of the rate performance of the monodispersed $LiFePO_4$@C core–shell structures and the $LiFePO_4$/C composites, whereby rates of up to 30 C have been employed. Compared with $LiFePO_4$/C composites, the monodispersed $LiFePO_4$@C core–shell structures not only exhibits higher discharge capacities at the low rate of 0.1 C but also with the rate changing from 0.1 to 30 C maintains steady in discharge capacity with an unconspicuous descent. At the rate of 0.1 C, the discharge capacity of $LiFePO_4$@C is ca. 145 mAh $g^{-1}$. The reversible specific capacity of $LiFePO_4$@C remains approximately 129 mAh $g^{-1}$ at 10 C charge/discharge rate and 112 mAh $g^{-1}$ at 30 C charge/discharge rate. Moreover, as long as the current density reverses back to the initial rate of 0.1 C, the positive electrode can retain the original discharge capacity of 145 mAh $g^{-1}$. The rate performance of the monodispersed $LiFePO_4$@C core–shell nanostructures is almost equal to that of the $LiFePO_4$/carbon nanocomposites with a core–shell structure designed via an in situ polymerization restriction method by Wang et al. [10], while is better than that of the monodispersed porous $LiFePO_4$/C/PPy microspheres synthesized by Sun et al. using a solvothermal method with EG as solvent and assisted with some organic modifiers [12]. Fig. 4d further exhibits the charge/discharge profiles of $LiFePO_4$@C at different rate of 0.1, 1, 5, 20, and 30 C. The long plat plateaus illustrate the charge and discharge capacities are predominated by the two-phase reaction, $LiFePO_4 \leftrightarrow (1-x)\,LiFePO_4 + x\,FePO_4 + x\,Li^+ + x\,e^-$, whether at low rate of 0.1 C or at high rate of 30 C. Moreover, due to the very small polarization resulted from the excellent kinetics the voltage difference between the discharge flat plateau and the charge flat plateau of $LiFePO_4$@C is very small only achieves 100 mV even at the rate of 30 C. Fig. 4e displays the long-time cycle performance of the monodispersed $LiFePO_4$@C core–shell nanostructures at the rate of 1 C. Although

the $LiFePO_4$@C initially has a slightly reduced discharge-specific capacity, it shows fascinating cycle stability. After 100 cycles, the discharge capacity still achieves 139 mAh $g^{-1}$, which corresponds to 98% capacity retention of the initial discharge capacity of 142 mAh $g^{-1}$ and 82% of the theoretical capacity of 170 mAh $g^{-1}$.

The excellent rate and cycle performance of the monodispersed $LiFePO_4$@C core–shell nanostructures may be ascribed to the fast reaction and ionic diffusion kinetics of the well-crystallized nanosized $LiFePO_4$ particles, and the good electronic contact by the full carbon-coating shell. Due to the reducing effects of EG and ascorbic acid, the oxidization of $Fe^{2+}$ to $Fe^{3+}$ is effectively suppressed, resulting in the solvothermally synthesized $LiFePO_4$ nanopillows are of high perfect olivine crystal structure. Moreover, the olivine crystal structure of $LiFePO_4$ is further improved during the decomposition of the ascorbic acid at high temperature for the formation of the full carbon-coating, facilitating the fast reaction and ionic diffusion. On the other hand, the full carbon-coating, which ensures the $LiFePO_4$ particle gets electrons from all directions, could further alleviate the polarization phenomenon in view of the one-dimensional $Li^+$ ion mobility in the framework [40]. Under the synergistic effect of the full carbon-coating and the well-crystallized nanosized particles, the monodispersed $LiFePO_4$@C core–shell nanostructures are of very low polarization and high kinetics, and exhibit nice capacity retention and high rate capacity. However, due to the obvious polarization and poor kinetics brought about from the partial carbon-coating and the weakening reducing effect, the $LiFePO_4$/C composites prepared with the hydrothermally synthesized $LiFePO_4$ display poor rate and cycle performance.

## 4. Conclusions

In summary, a facile two-step process has been developed for preparing monodispersed $LiFePO_4$@C core–shell nanostructures in high yield. The solvothermal synthesis of the monodispersed $LiFePO_4$ nanopillows with EG as reaction medium solvent is the basis. After a mixture and a thermal decomposition of the carbon-containing precursor of ascorbic acid with the monodispersed $LiFePO_4$ nanoparticles, the monodispersed $LiFePO_4$@C core–shell nanostructures are obtained. EG as the solvothermal reaction medium solvent plays an important role in the synthesis of the monodispersed $LiFePO_4$ nanopillows. The pouring nucleation brought about from the very small volume fraction of water in the feedstock and the adsorption of EG by hydrogen bonding leads to the formation of the monodispersed $LiFePO_4$ nanoparticles. The full carbon-coating ensures the $LiFePO_4$ nanoparticle gets electrons from all directions and further effectively alleviates the polarization phenomenon. This feature, combined with the well perfect olivine crystal structure, results in the electrodes of high rate capacity and excellent cycle performance. From a more fundamental point of view, we believe that the proposed approach in the present work shows a promising technique to prepare positive cathode materials with nice capacity retention and high rate capacity in high yield.

## Acknowledgement

This work is supported by the National Natural Science Foundation of China, under Grant Nos. 61274004 and 51232006, the Zhejiang Natural Science Foundation, China, under Grant No. LY12B07007, and Key Science and Technology Innovation Team of Zhejiang Province under grant number 2010R50013.

## Appendix A. Supplementary data

Supplementary data related to this article can be found at http://dx.doi.org/10.1016/j.jpowsour.2013.07.089.

## References

[1] A.K. Padhi, K.S. Nanjundaswamy, J.B. Goodenough, J. Electrochem. Soc. 144 (1997) 1188.
[2] J.M. Tarascon, M. Armand, Nature 414 (2001) 359–367.
[3] B.L. Ellis, K.T. Lee, L.F. Nazar, Chem. Mater. 22 (2010) 691–714.
[4] P.S. Herle, B. Ellis, N. Coombs, L.F. Nazar, Nat. Mater. 3 (2004) 147.
[5] S.Y. Chung, J.T. Bloking, Y.M. Chiang, Nat. Mater. 1 (2002) 123–128.
[6] Y.S. Hu, Y.G. Guo, R. Dominko, M. Gaberscek, J. Jamnik, J. Maier, Adv. Mater. 19 (2007) 1963–1966.
[7] R. Amin, P. Balaya, J. Maier, Electrochem. Solid-State Lett. 10 (2007) A13–A16.
[8] Y. Shi, S.L. Chou, J.Z. Wang, D. Wexler, H.J. Li, H.K. Liu, Y.P. Wu, J. Mater. Chem. 22 (2012) 16465–16470.
[9] X.F. Zhou, F. Wang, Y.M. Zhu, Z.N. Liu, J. Mater. Chem. 21 (2011) 3353–3358.
[10] Y.G. Wang, Y.R. Wang, E. Hosona, K. Wang, H.S. Zhou, Angew. Chem. Int. Ed. 47 (2008) 7461–7465.
[11] H. Nakano, K. Dokko, S. Koizumi, H. Tannai, K. Kanamura, J. Electrochem. Soc. 155 (2008) A909–A914.
[12] C.W. Sun, S. Rajasekhara, J.B. Goodenough, F. Zhou, J. Am. Chem. Soc. 133 (2011) 2132–2135.
[13] S. Yoon, C. Liao, X.G. Sun, C.A. Bridges, R.R. Unocic, J. Nanda, S. Dai, M.P. Paranthaman, J. Mater. Chem. 22 (2012) 4611–4614.
[14] J.D. Wilcox, M.M. Doeff, M. Marcinek, R. Kostecki, J. Electrochem. Soc. 154 (2007) A389.
[15] X.L. Wu, L.Y. Jiang, F.F. Cao, Y.G. Guo, L.J. Wan, Adv. Mater. 21 (2009) 2710–2714.
[16] J.F. Ni, M. Morishita, Y. Kawabe, M. Watada, N. Takeichi, T. Sakai, J. Power Sources 195 (2010) 2877–2882.
[17] X. Qin, X.H. Wang, H. Xiang, J. Xie, J. Li, Y. Zhou, J. Phys. Chem. C 114 (2010) 16806–16812.
[18] Y. Zhang, W. Wang, P. Li, Y. Fu, X. Ma, J. Power Sources 210 (2012) 47–53.
[19] Z.D. Huang, S.W. Oh, Y.B. He, B. Zhang, Y. Yang, Y.W. Mai, J.K. Kim, J. Mater. Chem. 22 (2012) 19643–19645.
[20] A.A. Salah, A. Mauger, K. Zaghib, J.B. Goodenough, N. Ravet, M. Gauthier, F. Gendron, C.M. Julien, J. Electrochem. Soc. 153 (2006) A1692–A1701.
[21] S. Franger, F.L. Cras, C. Bourbon, H. Rouault, J. Power Sources 119 (2003) 252–257.
[22] S.J. Kwon, C.W. Kim, W.T. Jeong, K.S. Lee, J. Power Sources 137 (2004) 93–99.
[23] C. Delacourt, P. Poizot, S. Levasseur, C. Masquelier, Electrochem. Solid-State Lett. 9 (2006) A325–A355.
[24] K.F. Hsu, S.Y. Tsay, B.J. Hwang, J. Mater. Chem. 14 (2004) 2690–2695.
[25] J. Yang, J.J. Xu, Electrochem. Solid-State Lett. 7 (2004) A515–A518.
[26] S.W. Oh, Z.D. Huang, B. Zhang, Y. Yu, Y.B. He, J.K. Kim, J. Mater. Chem. 22 (2012) 17215–17221.
[27] D.H. Kim, J.K. Kim, Electrochem. Solid-State Lett. 9 (2006) A439–A442.
[28 ] S.F. Yang, P.Y. Zavalij, M.S. Whittingham, Electrochem. Commun. 3 (2001) 505–508.
[29] J. Chen, M.J. Vacchio, S. Wang, N. Chernova, P.Y. Zavalij, M.S. Whittingham, Solid State Ionics 178 (2008) 1676–1693.
[30] G. Meligrana, C. Gerbaldi, A. Tuel, S. Bodoardo, N. Penazzi, J. Power Sources 160 (2006) 516–522.
[31] B. Ellis, W.H. Kan, W.R.M. Makahnouk, L.F. Nazar, J. Mater. Chem. 17 (2007) 3248–3254.
[32] G. Xu, X. Yang, C.X. Hua, J.H. He, Z.H. Ren, W.J. Weng, P.Y. Du, G. Shen, G.R. Han, CrystEngComm 14 (2012) 6783–6787.
[33] G. Xu, W.B. He, Y.G. Zhao, Y. Liu, Z.H. Ren, G. Shen, G.R. Han, CrystEngComm 13 (2011) 1498–1503.
[34] D. Rangappa, K. Sone, T. Kudo, I. Honma, J. Power Sources 195 (2010) 6167–6171.
[35] F. Teng, S. Santhanagopalan, A. Asthana, X. Geng, S. Mho, R. Shahbazian-Yassar, D.D. Meng, J. Cryst. Growth 312 (2010) 3493–3502.
[36] F. Teng, S. Santhanagopalan, R. Lemmens, X. Geng, P. Patel, D.D. Meng, Solid State Sci. 12 (2010) 952–955.
[37] C. Nan, J. Lu, C. Chen, Q. Peng, Y. Li, J. Mater. Chem. 21 (2011) 9994.
[38] E.P. Stambaugh, Hydrothermal Precipitation of High-quality Oxides, 1977. Presented at the SME-AIME Fall Meeting St. Louis, MO, USA.
[39] G. Garnweitnei, J. Hentschel, M. Antonietti, M. Niederberger, Chem. Mater. 17 (2005) 4594–4599.
[40] D. Morgan, A. Van Der Ven, G. Ceder, Electrochem. Solid-State Lett. 7 (2004) A30–A32.